In-Situ X-ray Absorption Spectroscopic Study on Variation of Electronic Transitions and Local Structure of $LiNi_{1/3}Co_{1/3}Mn_{1/3}O_2$ Cathode Material during Electrochemical Cycling

Y. W. Tsai,[†] B. J. Hwang,*,[†,‡] G. Ceder,[‡] H. S. Sheu,[§] D. G. Liu,[§] and J. F. Lee[§]

Nanoelectrochemical Laboratory, Department of Chemical Engineering, National Taiwan University of Science and Technology, Section 4, #43, Keelung Road, Taipei 106, Taiwan, Republic of China, Department of Materials Science and Engineering and Center for Materials Science and Engineering, Massachusetts Institute of Technology, Cambridge, Massachusetts 02139-4307, and National Synchrotron Radiation Research Center, #101, Hsin-Ann Road, Science-Based Industrial Park, Hsinchu 30077, Taiwan, Republic of China

In-situ X-ray absorption spectroscopic investigations have been carried out to examine the changes of the electronic transitions and local structure at the Mn, Co, and Ni K-edge for the $LiNi_{1/3}Co_{1/3}Mn_{1/3}O_2$ electrode during charging and discharging process in this study. It was found that only Ni atom in $Li_{1-x}Ni_{1/3}Co_{1/3}Mn_{1/3}O_2$ is electroactive from the evolution of the XANES spectra and the bond length variation of Ni−O. It was found that the redox pairs of Ni^{2+}/Ni^{3+} and Ni^{3+}/Ni^{4+} exist and the oxidation states of Mn and Co remain as Mn^{IV} and Co^{III}, respectively, in $Li_{1-x}Ni_{1/3}Co_{1/3}Mn_{1/3}O_2$ upon charge and discharge. The oxygen, rather than the transition-metal ions (Ni, Co, and Mn), functions as electron donor at the end of charge. In addition, the irreversible capacity at the first cycle derives mainly from the appearance of inactive Ni, which is evidenced by the energy shift $E - E_0$ of the absorption edge for the Ni absorber and the bond length change of the Ni−O. A decrease/increase of Debye−Waller factor of Ni−O contribution results from a decrease/increase of Jahn−Teller active Ni^{III} concentration during cycling. The trends of the variations for the bond length and Debye−Waller factor for the second shell Mn−M and Ni−M contributions are significant and similar, suggesting the short-range ordering between Ni^{II} and Mn^{IV} may take place in this compound.

Introduction

$LiCoO_2$ is currently being used as a cathode material in commercial lithium ion batteries because of its easy synthesis and good cyclability. However, this material is expensive and the practically attainable rechargeable capacity is only 50% (140 mAh/g) of the theoretical capacity (274 mAh/g). $LiNiO_2$ is considerably less expensive and has a higher initial capacity (200 mAh/g) than $LiCoO_2$.[1] However, this material is known to be more difficult to synthesize and suffers from poor cyclability. Partial substitution of Ni by other metal cations has been made to enhance the $LiNiO_2$ electrochemical performance.[2] In particular, the solid solution, $LiNi_{1-x}Co_xO_2$, has been suggested as an alternative to $LiNiO_2$ as it combines some of the benefits of $LiNiO_2$ (capacity) with those of $LiCoO_2$ (stability).[3] Substitution of Ni by lower cost metals, such as Mn, has also been investigated.[4] Results of Liu et

al.[5] and Tsai et al.[6] indicate that Mn is effective in improving initial capacity and cycle life of lithium nickel cobalt oxide. Recently, a series of $LiNi_xCo_{1-2x}Mn_xO_2$ compounds ($0 \leq x \leq 1/2$) becomes of great interest.[7] $LiNi_{1/3}Co_{1/3}Mn_{1/3}O_2$ shows the best cell performance among the compounds. $LiNi_{1/3}Co_{1/3}Mn_{1/3}O_2$ synthesized by a solid-state method has been reported to have a capacity of 150 mAh/g in the voltage window of 2.5−4.2 V by Ohzuku and Makimura.[8] A capacity of 200 mAh/g in the voltage window of 2.5−4.6 V has also been reported by Yabuuchi and Ohzuku.[9] In our previous paper,[10] we have demonstrated that $LiNi_{1/3}Co_{1/3}Mn_{1/3}O_2$ synthesized by a sol−gel method shows the initial discharge capacity of 188 mAh/g and good capacity retention. The electronic transition and local structure of $LiNi_{1/3}Co_{1/3}Mn_{1/3}O_2$ have been investigated using first principles calculation.[10,11]

The ordering of the ions in the transition metal layer of $LiNi_{0.5}Mn_{0.5}O_2$ and $Li[Ni_xMn_{(2-x)/3}Li_{(1-2x)/3}]O_2$ compounds is

* Corresponding author. E-mail: bjh@ch.ntust.edu.tw.
† National Taiwan University of Science and Technology.
‡ Massachusetts Institute of Technology.
§ National Synchrotron Radiation Research Center.
(1) Ohzuku, T.; Ueda, A.; Nagayama, M. *J. Electrochem. Soc.* **1993,** *140,* 1862.
(2) Delmas, C.; Saadoune, I.; Rougier, A. *J. Power Sources* **1993,** *43/44,* 595.
(3) Hwang, B. J.; Santhanam, R.; Chen, C. H. *J. Power Sources* **2003,** *114,* 244.
(4) Winter, M.; Besenhard, J. O.; Spahr, M. E.; Novak, P. *Adv. Mater.* **1998,** *10,* 725.

(5) Liu, Z.; Yu, A.; Lee, J. Y. *J. Power Sources* **1999,** *81−82,* 416.
(6) Hwang, B. J.; Santhanam, R.; Chen, C. H.; Tsai, Y. W. *J. Mater. Chem.* **2003,** *13,* 1962.
(7) MacNeil, D. D.; Lu, Z.; Dahn, J. R. *J. Electrochem. Soc.* **2002,** *149,* A1332.
(8) Ohzuku, T.; Makimura, Y. *Chem. Lett.* **2001,** 642.
(9) Yabuuchi, N.; Ohzuku, T. Extended abstract No. 122, IMLB 11, June 23−28, Monterey, USA, 2002.
(10) Hwang, B. J.; Tsai, Y. W.; Carlier, D.; Ceder, G. *Chem. Mater.* **2003,** *15,* 3676.
(11) Koyama, Y.; Tanaka, I.; Adachi, H.; Makimura, Y.; Ohzuku, T. Extended abstract No. 183, IMLB 11, June 23−28, Monterey, USA, 2002.

of great interest because these materials show anomalously high capacity. Recent computational[12] and NMR[13] studies provide information about short-range ordering in the transition metal layer of these compounds. The short-range ordering between Ni and Mn ions in the $LiNi_{0.65}Co_{0.25}Mn_{0.1}O_2$ compound has also been observed from extended X-ray absorption fine structure (EXAFS) studies.[14] It is of great essence to understand if short-range ordering exists in $LiNi_{1/3}Co_{1/3}Mn_{1/3}O_2$ material.

The purpose of this paper is to investigate the variation of oxidation states and local structure by in-situ X-ray absorption spectroscopy (XAS) upon delithiation and lithiation. It can provide a fundamental understanding of the charging−discharging mechanism and short-range ordering in the transition layers of the $LiNi_{1/3}Co_{1/3}Mn_{1/3}O_2$ material.

Experimental Section

Synthesis and Fabrication. Layered $LiNi_{1/3}Co_{1/3}Mn_{1/3}O_2$ compound with pure $R\bar{3}m$ symmetry was successfully synthesized by a sol−gel method. A stoichiometric amount of the starting materials $Li(CH_3COO)\cdot2H_2O$, $Ni(CH_3COO)_2\cdot4H_2O$, $Co(NO_3)_2\cdot6H_2O$, and $Mn(CH_3COO)_2\cdot4H_2O$ was dissolved in distilled water and then mixed with citric acid as a chelating agent. The solution was stirred at 80−90 °C for 5−6 h to form the clear viscous gel, and then the precursor was obtained by drying in a vacuum oven at 140 °C for 24 h. $LiNi_{1/3}Co_{1/3}Mn_{1/3}O_2$ powder was ground and calcined at 900 °C for 12 h after precalcining the obtained precursor at 450 °C. The temperature ramp for heating and cooling was fixed at 2 °C/min.

The crystal structure for $Li_{1-x}Ni_{1/3}Co_{1/3}Mn_{1/3}O_2$ as a function of x was studied by powder X-ray diffraction technique using the synchrotron radiation light source with the wavelength of 1.3215 Å at the beam line of BL17A of National Synchrotron Radiation Research Center (NSRRC), in Hsinchu of Taiwan. The energy of the light source into the hutch was adjusted to be 9 keV through the monochromator Si(111), and the spot of the optics is focused into the area of 1 mm × 3 mm by the entrance slits. All of the XRD patterns were collected by a flat image plate with the area of 20 cm × 40 cm (Fuji-film Ltd.) and then read out by using a MAC IPR420 off line imaging plate scanner. The 2θ scan was performed in the range of 10°−60° with the step size of 0.02°.

The in-situ coin-cell, composed of $LiNi_{1/3}Co_{1/3}Mn_{1/3}O_2$ as a cathode, lithium metal (FMC) as an anode, and PE as a separator, was used to conduct in-situ X-ray absorption measurements during charge and discharge processes. 1.0 M $LiPF_6$ dissolved in a 1:1 mixture of ethylene carbonate (EC)/diethyl carbonate (DEC) was used as an electrolyte. All of the coin cells were assembled in an argon-filled drybox where both moisture and oxygen content were less than 1 ppm. The electrochemical characterization of the $LiNi_{1/3}Co_{1/3}Mn_{1/3}O_2$ electrode was performed at 0.1 C-rate over a potential range between 3.0 and 4.5 V upon the charge and discharge.

X-ray Absorption Spectroscopy Measurement. In-situ X-ray absorption spectra (XAS) were collected at the beam line BL17C of National Synchrotron Radiation Research Center (NSRRC) at Hsinchu, Taiwan. The storage ring of the electronic accelerator can supply the electronic energy of 1.5 GeV and the operation current

between 100 and 200 mA. A Si double crystal monochromator was used to perform energy scan, of which the parallelism can be adjusted to eliminate the high order harmonics. All XAS data were recorded using the transmission mode. The ionization chambers were applied as detectors to monitor the intensity of the incident and transmitted beams through the specimen. The absorption coefficient can be calculated from the logarithm of the intensity ratio of the incident and transmitted beams. The references Mn, Co, and Ni metal foils were positioned in front of the window of the third ionization chamber and measured simultaneously as a standard energy for calibration in each energy scan. The beam size was limited by the horizontal and vertical slits with the area of 2 × 2 mm^2 during in-situ XAS measurements. For pristine $LiNi_{1/3}Co_{1/3}Mn_{1/3}O_2$ electrode, the edge jumps for different absorbers were determined from the XANES spectra, which show 0.82, 0.63, and 0.60 for Mn, Co, and Ni K-edges, respectively.

EXAFS Data Analysis. The EXAFS data were analyzed by the standard procedures shown as follows. First, a linear function was applied to fit the background in the pre-edge region of the raw absorption spectrum. A cubic spline was used to find out the smooth oscillation curve as a background of the spectrum above the absorption edge. The EXAFS function χ was obtained by subtracting the postedge background from the overall absorption and then normalized with respect to the edge jump step. The normalized $\chi(E)$ was transformed from energy space to k space, where k is the photoelectron wave vector. The $\chi(k)$ data could be obtained to describe the oscillation of backscattering wave through the local environment about ∼10 Å. For $LiNi_{1/3}Co_{1/3}Mn_{1/3}O_2$ cathode material, the k^2-weighted EXAFS spectra, $k^2\cdot\chi(k)$, for the selected absorber Mn, Co, and Ni, were calculated to compensate the damping of EXAFS oscillations in high-k region. Subsequently, k^2-weighted $\chi(k)$ data in the k-space ranging from 3.67 to 11.4 $Å^{-1}$ for Mn K-edge, 3.55−12.15 $Å^{-1}$ for Co K-edge, and 3.45−14.0 $Å^{-1}$ for Ni K-edge, respectively, were Fourier transformed (FT) to r-space to separate the EXAFS contributions from different coordination shells. A nonlinear least-squares algorithm was applied for curve fitting of EXAFS in r-space between 0.73 and 5.61 $Å^{-1}$ for Mn K-edge, 0.67 and 5.65 Å for Co K-edge, and 0.71 and 5.68 $Å^{-1}$ for Ni K-edge, respectively.

The structure parameters for specific absorber, such as coordination numbers (N), bond distances (R), and Debye−Waller factor (σ^2), were extracted by curve fitting analysis based on FEFFIT. The theoretical EXAFS parameters, backscattering amplitude and phase shift, were calculated by FEFF7 code for all possible scattering paths, which were generated from the crystallographic model of the known structures. The amplitude reduction factor S_0^2 was scaled to a fixed value of 0.67, 0.74, and 0.81 for Mn, Co, and Ni absorbers, respectively, after preliminary refinements. The coordination numbers (N) were also fixed to the crystallographic values because the N value is highly correlated with the Debye−Waller factor. (Note that the coordination number was fixed as 6 for the first shell M−O, 6 for the second shell M−M, 12 for the third shell M−M involving atoms within the intralayer and two adjacent metal layers, and 12 for the fourth shell M−M−M with linear ordering, respectively. M represents Mn, Co, and Ni absorbers.)

Results and Discussion

Ex-Situ X-ray Diffraction Patterns. The XRD patterns for the layered $Li_{1-x}Ni_{1/3}Co_{1/3}Mn_{1/3}O_2$ cathode materials with different lithium contents are given in Figure 1, indicating that all of the $Li_{1-x}Ni_{1/3}Co_{1/3}Mn_{1/3}O_2$ samples have the typical layered structure of α-NaFeO$_2$ type with space group $R\bar{3}m$, where the Li atoms are occupied at 3a (0, 0, 0) site in the

(12) Van der Ven, A.; Ceder, G. *Electrochem. Commun.*, in press.
(13) Yoon, W.-S.; Iannopollo, S.; Grey, C. P.; Caelier, D.; Gorman, J.; Reed, J.; Ceder, G. J. *Electrochem. Solid-State Lett.* **2004**, *7*, A167.
(14) Tsai, Y. W.; Hwang, B. J.; Liu, D. G.; Lee, J. F. *J. Mater. Chem.* **2004**, *14*, 958.

LiNi$_{1/3}$Co$_{1/3}$Mn$_{1/3}$O$_2$ Cathode Material

Chem. Mater., Vol. 17, No. 12, 2005 3193
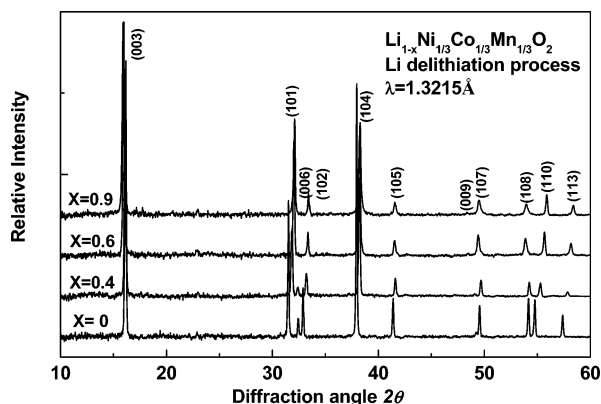
Figure 1. Ex-situ XRD patterns with the wavelength λ of 1.3215 Å for Li$_{1-x}$Ni$_{1/3}$Co$_{1/3}$Mn$_{1/3}$O$_2$ at different delithiation states.

Table 1. Variation of Lattice Parameters *a,c* and Cell Volume for Li$_{1-x}$Ni$_{1/3}$Co$_{1/3}$Mn$_{1/3}$O$_2$ at Different Delithiation States

Li$_{1-x}$Ni$_{1/3}$Co$_{1/3}$Mn$_{1/3}$O$_2$	lattice parameters			
	a (Å)	*c* (Å)	*c/a*	cell volume (Å^3)
$x = 0$	2.864(4)	14.247(27)	4.97	101.20(31)
$x = 0.4$	2.843(5)	14.285(34)	5.02	100.05(38)
$x = 0.6$	2.825(5)	14.471(38)	5.12	100.02(38)
$x = 0.9$	2.815(4)	14.503(31)	5.15	99.5(30)

lithium layer, the Ni/Co/Mn atoms are positioned at 3b (0, 0, 0.5) site in the transition metal layer, and the O atoms are located at 6c (0, 0, 0.24) site in the edge-shared MO$_6$ octahedra. The Li ions are placed in the interstitial channel surrounded by the edge-shared faces of MO$_6$ octahedra within the *ab* planes. The unit-cell parameters calculated from the Rietveld refinement of the XRD patterns for the Li$_{1-x}$Ni$_{1/3}$Co$_{1/3}$Mn$_{1/3}$O$_2$ electrodes with different lithium contents are shown in Table 1. The lattice parameters *a* and *c* in the pristine compound of LiNi$_{1/3}$Co$_{1/3}$Mn$_{1/3}$O$_2$ are determined to be 2.864 and 14.247 Å, respectively. These data match well with the values observed by Ohzuku and Makimura[8] (*a* = 2.867 Å and *c* = 14.246 Å) and Shaju et al.[15] (*a* = 2.864 Å and *c* = 14.233 Å). The lattice parameters *a* and *c* were given to be 2.892 and 14.251 Å, respectively, from first principles calculation in our previous paper. The experimental values are slightly smaller than those calculated, as is often the case for computations in the generalized gradient approximation.[10] The experimental lattice parameter *a* and *c* decreases and increases, respectively, with an increase in the *x* values, indicating that the lithium extraction leads to the shrinkage of interatomic distance with the *ab* plane and the increase of the interplanar distance between *ab* planes. The increase of interplanar distance is due to the electrostatic repulsion between *ab* planes by the removal of Li ions. Although X-ray diffraction is a powerful technique to provide the detailed information of the long-range structure of materials, it is difficult to investigate the change of the oxidation states and local structure of materials upon charging and discharging processes. In-situ X-ray absorption measurements were applied to examine the variations of the oxidation states and local structure surrounding the target atoms of the LiNi$_{1/3}$Co$_{1/3}$Mn$_{1/3}$O$_2$ compound during charge and discharge processes.

(15) Shaju, K. M.; Subba Rao, G. V.; Chowdari, B. V. R. *Electrochim. Acta* **2002**, *48*, 145.
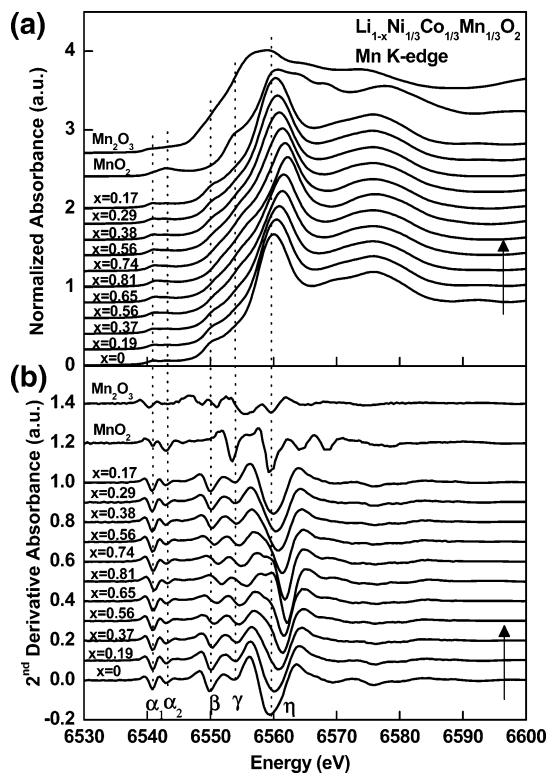
Figure 2. (a) Normalized absorbance and (b) second derivative absorbance of Mn K-edge for Li$_{1-x}$Ni$_{1/3}$Co$_{1/3}$Mn$_{1/3}$O$_2$ at different lithium contents during first charge and discharge cycle.

In-Situ Electrochemical Characterization. To elucidate the changes of the electronic transitions and local structure of the layered LiNi$_{1/3}$Co$_{1/3}$Mn$_{1/3}$O$_2$ material, in-situ X-ray absorption observations at Mn, Co, and Ni K-edges were carried out during the first cycle. The in-situ cell of LiNi$_{1/3}$Co$_{1/3}$Mn$_{1/3}$O$_2$/LiPF$_6$+EC+DEC/Li was cycled at 0.1 C in the potential range of 3 and 4.5 V (vs Li metal). It indicates that the charge and discharge capacities at the first cycle are 232.7 and 190 mAh/g, respectively. The irreversible capacity at the first cycle is found to be 42.7 mAh/g.

In-Situ X-ray Absorption Near-Edge Spectroscopy. The normalized and second derivative XANES spectra at the Mn, Co, and Ni K-edges for the Li$_{1-x}$Ni$_{1/3}$Co$_{1/3}$Mn$_{1/3}$O$_2$ compound as a function of *x* during charge and discharge processes, along with the reference compounds Mn$_2$O$_3$ (Mn^{3+}), MnO$_4$ (Mn^{4+}), CoO (Co^{2+}), LiCoO$_2$ (Co^{3+}), NiO (Ni^{2+}), and LiNiO$_2$ (Ni^{3+}) as formal valences, are given in parts (a) and (b) of Figures 2−4, respectively. The second derivative features of the Mn, Co, and Ni K-edges XANES spectra shown in Figures 2−4 are labeled by the small Greek letters α_1, α_2, α, β, γ, and η, indicating that the considerable electronic transitions around the selected atoms Mn, Co, and Ni exhibit in the Li$_{1-x}$Ni$_{1/3}$Co$_{1/3}$Mn$_{1/3}$O$_2$ compounds at different *x* values. That shows the electronic transitions from 1s core level to excited vacant bound states with appropriate symmetry. For the pristine Li$_{1-x}$Ni$_{1/3}$Co$_{1/3}$Mn$_{1/3}$O$_2$ compound ($x = 0$), the edge position for the Mn, Co, and Ni K-edges is almost the same as that of the references MnO$_2$(Mn^{4+}), LiCoO$_2$(Co^{3+}), and NiO(Ni^{2+}), as shown in Figures 2−4, respectively, suggesting that the oxidation states of the selected absorbing atoms are +4 for Mn, +3 for Co, and +2 for Ni in the pristine material. Although a rigorous assignment of XANES
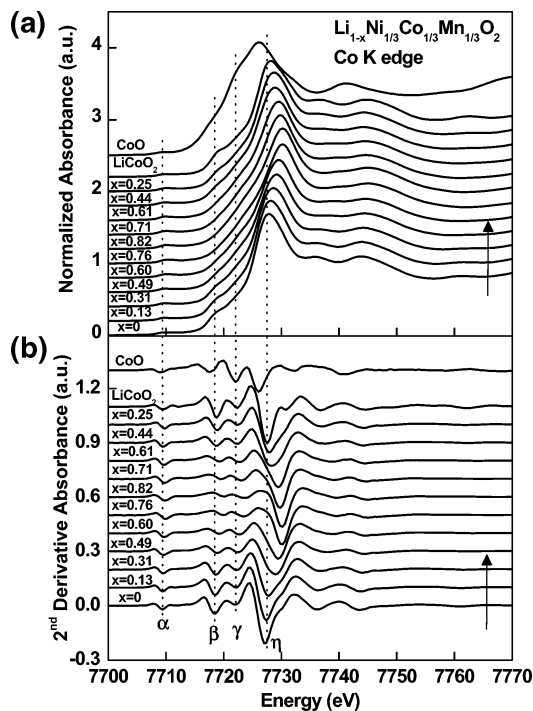
Figure 3. (a) Normalized absorbance and (b) second derivative absorbance of Co K-edge for $Li_{1-x}Ni_{1/3}Co_{1/3}Mn_{1/3}O_2$ at different lithium contents during first charge and discharge cycle.
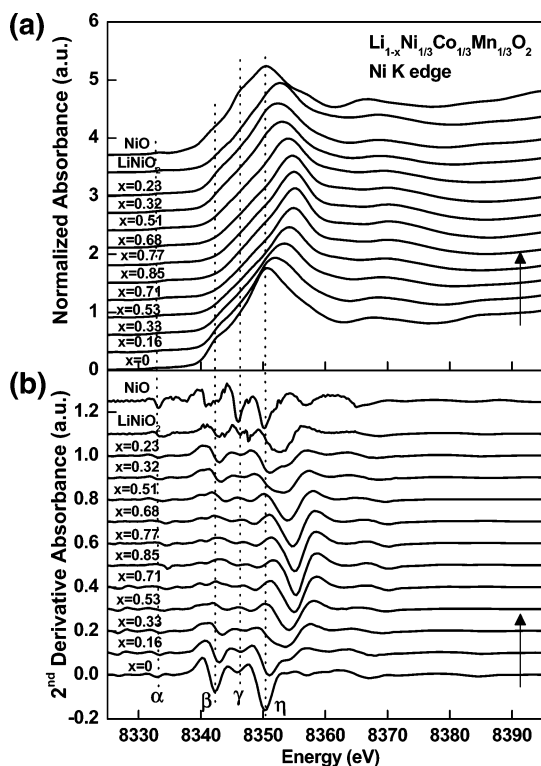
Figure 4. (a) Normalized absorbance and (b) second derivative absorbance of Ni K-edge for $Li_{1-x}Ni_{1/3}Co_{1/3}Mn_{1/3}O_2$ at different lithium contents during first charge and discharge cycle.

transition is difficult, especially in the absence of polarized spectra, each feature of XANES spectra can be interpreted in terms of the local geometry and local electronic structure of the Ni/Co/Mn ions.[16] The weak pre-edge absorption peak of α or (α_1 and α_2) in Figures 2−4 was assigned to be an

electronic excitation of 1s core state to unoccupied 3d orbital of high spin $Mn^{4+}(t_{2g}{}^3e_g{}^0)$, low spin $Co^{3+}(t_{2g}{}^6e_g{}^0)$, and low spin $Ni^{2+}(t_{2g}{}^6e_g{}^2)$ ions, respectively. Although the 1s → 3d transition is the formally electric dipole-forbidden transition in an ideal octahedral symmetry, the appearance of a weak absorption peak is due to the pure electric quadrupole coupling and/or the 3d−4p orbital mixing arising from the noncentrosymmetric environment of the slightly distorted octahedral 3a sites in the rhombohedral $R\bar{3}m$ space group.[17] The absorption peaks of β appear at the Mn, Co, and Ni K-edges. XANES spectra are due to the electric dipole-allowed transition of a 1s core electron to an unoccupied 4p bound state with T_{1u} symmetry.[16] The β peak at Figures 2−4 corresponds to the final states of $1s^1c3d^4L4p^1$, $1s^1c3d^7L4p^1$, and $1s^1c3d^9L4p^1$ for Mn^{4+}, Co^{3+}, and Ni^{2+}, respectively, with shakedown process originated from ligand-to-metal charge transfer (LMCT). Also, the main absorption peak η of the Mn, Co, and Ni K-edges XANES spectra was treated as a purely dipole-allowed 1s→4p transition without shakedown process, which matches the final state of $1s^1c3d^34p^1$ for Mn^{4+}, $1s^1c3d^64p^1$ for Co^{3+}, and $1s^1c3d^84p^1$ for Ni^{2+}, respectively. Herein, the c and L denote a 1s core hole and an oxygen 2p ligand hole, respectively. The absorption peak β demonstrates the energy position lower than the absorption peak ϵ, because the 1s core electron ascribed to the charge-transfer on the more screened nucleus shows the bounded energy lower than that of the combined transitions relative to the unscreened excitation.[18]

While the Li ions were extracted or reinserted from/into the $LiNi_{1/3}Co_{1/3}Mn_{1/3}O_2$ compound, the in-situ Mn K-edge XANES spectra were obtained, as shown in Figure 2. The Mn K-edge XANES features exhibit some changes in the shape of the edge due to the changes in the Mn local environment but do not show the changes of the edge energy position upon charge and discharge. Particularly, the energy position of the peaks α_1 and α_2 is invariant at various states of charge and discharge, implying that the oxidation state of the absorbing atom Mn remains as +4 throughout charge and discharge. The intensity of the two peaks β and η, corresponding to 1s → 4p transitions with shakedown process and without shakedown process, become weak gradually upon charge due to the small decrease of p character by Mn 3d−4p orbital mixing. These feature variations of the Mn absorption edge at various states of charge are similar to those for $LiNi_{0.65}Co_{0.25}Mn_{0.1}O_2$,[14] $LiNi_{0.5}Mn_{0.5}O_2$,[17] and $Li_{1.2}$-$Cr_{0.4}Mn_{0.4}O_2$[19] compounds. All of the XANES shape change of the Mn absorption edge is mainly caused by the variation of local structure during Li ions deintercalation and intercalation.

The successive changes of the Co K-edge XANES spectra for $Li_{1-x}Ni_{1/3}Co_{1/3}Mn_{1/3}O_2$ as a function of lithium contents upon charge and discharge are given in Figure 3. As Li ions deintercalate, the absorption intensities of two peaks β and

(16) Kim, M. G.; Yo, C. H. *J. Phys. Chem. B* **1999**, *103*, 6457.

(17) Yoon, W.-S.; Grey, C. P.; Balasubramanian, M.; Yang, X.-Q.; McBreen, J. *Chem. Mater.* **2003**, *15*, 3161.
(18) Tranquada, J. M.; Heald, S. M.; Moodenbaugh, A. R. *Phys. Rev. B* **1987**, *36*, 5263.
(19) Ammundsen, B.; Paulsen, J.; Davidson, I.; Liu, R. S.; Shen, C. H.; Chen, J. M.; Jang, L. Y.; Lee, J. F. *J. Electrochem. Soc.* **2002**, *149*, A431.

η show a systematic decrease upon charge because of the distorted CoO$_6$ structure associated with the small decrease of p character by Co 3d−4p orbital mixing. Also, the ϵ peak shifts toward high energy with an increase in the x values. The energy positions of the pre-edge peak α and the absorption edge for Co absorber show insignificant variations during Li ions extraction and reinsertion, indicating that the Co absorber remains the oxidation state of +3 and is inactive in the potential region of 3.0−4.5 V.

The systematic changes of the Ni K-edge XANES spectra as a function of x are presented in Figure 4. The energy positions of the pre-edge peak α and the absorption edge β of the Ni absorber for Li$_{1-x}$Ni$_{1/3}$Co$_{1/3}$Mn$_{1/3}$O$_2$ with $x = 0$ are similar to those of the reference NiO. Upon delithiation, these peaks gradually shift toward higher values and ultimately reach absorption energies higher than those in LiNiO$_2$ for $x > 0.85$. These peaks reversibly shift back to lower energy upon lithiation. This suggests that the redox pair reactions, either a two-step reaction of Ni^{2+}/Ni^{3+} and then Ni^{3+}/Ni^{4+} or a one-step reaction of Ni^{2+}/Ni^{4+}, might take place during charge and discharge cycle. The existence of Ni^{3+} during cycling will be further confirmed by EXAFS studies. Therefore, it suggests that the redox process is a two-step reaction, Ni^{2+}/Ni^{3+} and then Ni^{3+}/Ni^{4+}. The XANES feature for the Ni K-edge at $x = 0.33$, which agrees very well with that of the reference LiNiO$_2$, corresponds to a transition state from Ni^{2+} to Ni^{3+} upon charge. Also, the feature is nearly the same at $x = 0.32$ upon discharge. It was found that Ni^{2+} and Ni^{3+} ions coexist in the LiNi$_{1/3}$Co$_{1/3}$Mn$_{1/3}$O$_2$ material at the end of discharge, which is consistent with the irreversible absorption energy shift at Ni K-edge after the first cycle. It indicates that the irreversible capacity mainly results from a part of Ni^{3+} that cannot be reduced to Ni^{2+}.

The energy shift $E - E_0$ for Co and Ni K-edges at various states during cycle is indicated in Figure 5a and b, where E represents the energy position at half-height of the edge jump for the Co and Ni absorbers in the Li$_{1-x}$Ni$_{1/3}$Co$_{1/3}$Mn$_{1/3}$O$_2$ compound and E_0 means the energy position of absorption edge in which is 7717.5 eV for CoO and 8342.2 eV for NiO. As can be seen, the energy shift E $-$ E$_0$ for Co absorber in Li$_{1-x}$Ni$_{1/3}$Co$_{1/3}$Mn$_{1/3}$O$_2$ shows insignificant change and stays at 4 eV close to that in the reference LiCoO$_2$ (Co^{III}) during Li insertion and extraction. The oxidation state of the Co absorber remains as +3, implying the Co is almost inactive in Li$_{1-x}$Ni$_{1/3}$Co$_{1/3}$Mn$_{1/3}$O$_2$ during cycle in the potential range of 3−4.5 V. For the Ni absorber, the energy shift $E - E_0$ is 0 eV in the Li$_{1-x}$Ni$_{1/3}$Co$_{1/3}$Mn$_{1/3}$O$_2$ compound with $x = 0$, which is similar to that of NiO (Ni^{II}). A linear correlation of the energy shift $E - E_0$ for the Ni absorber in Li$_{1-x}$Ni$_{1/3}$Co$_{1/3}$Mn$_{1/3}$O$_2$ with respect to x upon delithiation and lithiation was shown in Figure 5b. The value of $E - E_0$ for the Ni absorber in Li$_{1-x}$Ni$_{1/3}$Co$_{1/3}$Mn$_{1/3}$O$_2$ with $x = 0.39$ shifts toward higher energy of 2.1 eV, which equals that of LiNiO$_2$, and then is 3.8 eV at the end of charge ($x = 0.84$). It is worth mentioning that the energy shift shows no more increase, which indicates the Ni^{2+} is completely oxidized while x is larger than 0.7. It shows good agreement with our computational results that the Ni^{2+} is predicted to be oxidized completely to Ni^{4+} at $x = 0.667$ in the Li$_{1-x}$Ni$_{1/3}$Co$_{1/3}$-
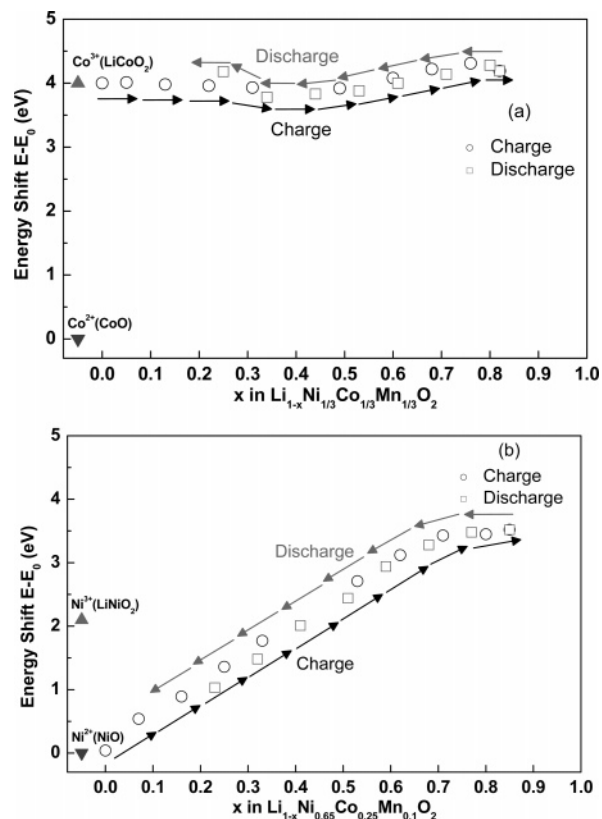
Figure 5. Energy shift $E - E_0$ of the Co (a) and Ni (b) K-edge at the half-height of the edge step for Li$_{1-x}$Ni$_{1/3}$Co$_{1/3}$Mn$_{1/3}$O$_2$ at different lithium contents during first charge and discharge cycle.

Mn$_{1/3}$O$_2$ compound. However, the oxidation states of all of the transition metal ions do not change significantly as x is larger than 0.7. It suggests that the oxygen, rather than the transition-metal ions (Ni, Co, and Mn), functions as electron donor at the end of charge, which is consistent with the experimental and computational observations in the literature.[13,20,21] The difference of $E - E_0$ for the Ni absorber between Li$_{1-x}$Ni$_{1/3}$Co$_{1/3}$Mn$_{1/3}$O$_2$ ($x = 0.85$) and the reference LiNiO$_2$ (Ni^{III}) is 1.8 eV, which is close to that (2.1 eV) between LiNiO$_2$ (Ni^{III}) and NiO(Ni^{II}), indicating that the redox reactions of Ni^{II}/Ni^{III} and Ni^{III}/Ni^{IV} take place in the Li$_{1-x}$Ni$_{1/3}$Co$_{1/3}$Mn$_{1/3}$O$_2$ upon delithiation and lithiation. As can be seen, the energy shift of the Ni absorber is going back to 1.4 eV instead of 0 eV at the end of discharge ($x = 0.25$), indicating the Ni^{4+} is not completely reduced to Ni^{2+}, which is responsible for the initial irreversible capacity at 0.1 C.

**In-Situ X-ray Absorption Fine Structure Spectroscopy.** The EXAFS experiment is a powerful technique to determine the changes of the local structure of the selected absorbers Mn, Co, and Ni for Li$_{1-x}$Ni$_{1/3}$Co$_{1/3}$Mn$_{1/3}$O$_2$ at different electrochemically Li delithiation or lithiation states. The k^2-weighted Fourier transformed spectra with the uncorrected phase and amplitude at the Mn, Co, and Ni K-edge for Li$_{1-x}$Ni$_{1/3}$Co$_{1/3}$Mn$_{1/3}$O$_2$ as a function of x are shown in Figures 6−8, respectively. The crystal structure of the LiNi$_{1/3}$Co$_{1/3}$-

(20) Aydinol, M. K.; Kohan, A. F.; Ceder, G.; Cho, K.; Joannopoulos, J. *Phys. Rev. B* **1997**, *56*, 1354.
(21) Ceder, G.; Chiang, Y. M.; Sadoway, D. R.; Aydinol, M. K.; Jang, Y. I.; Huang, B. *Nature* **1998**, *392*, 684.
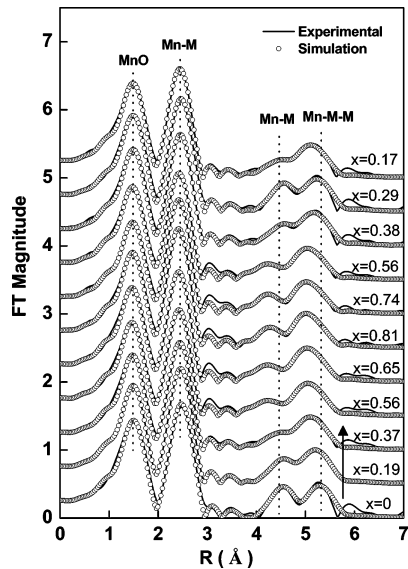
Figure 6. k^2-weighted FT spectra of Mn K-edge for $Li_{1-x}Ni_{1/3}Co_{1/3}Mn_{1/3}O_2$ at different lithium contents during first charge and discharge cycle.
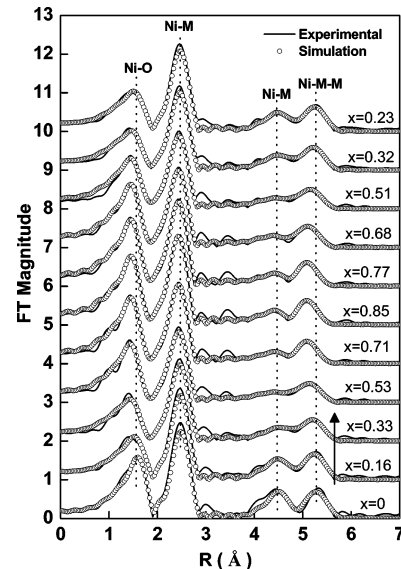
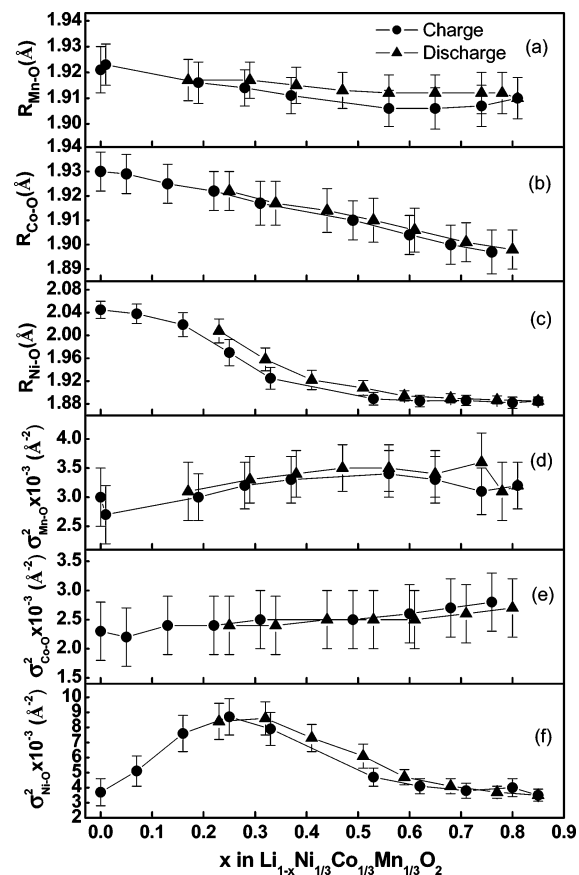**Figure 8.** k^2-weighted FT spectra of Ni K-edge for $Li_{1-x}Ni_{1/3}Co_{1/3}Mn_{1/3}O_2$ at different lithium contents during first charge and discharge cycle.
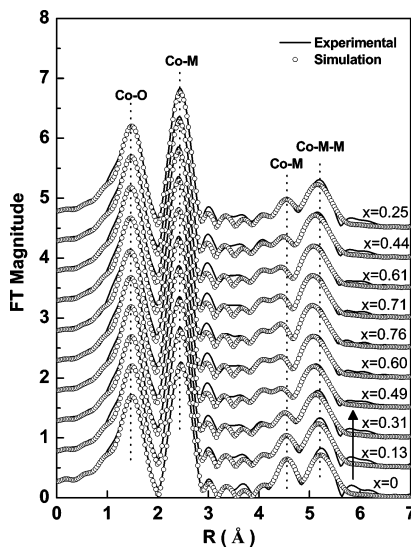
Figure 7. k^2-weighted FT spectra of Co K-edge for $Li_{1-x}Ni_{1/3}Co_{1/3}Mn_{1/3}O_2$ at different lithium contents during first charge and discharge cycle.

Figure 9. Structural parameter changes simulated at the first shell Mn−O, Co−O, and Ni−O for $Li_{1-x}Ni_{1/3}Co_{1/3}Mn_{1/3}O_2$ at different lithium contents during first charge and discharge cycle.

$Mn_{1/3}O_2$ compound confirmed by XRD is an ideal symmetry of hexagonal $R\bar{3}m$ space group. Four effective scattering paths ascribed to the single and multiple scattering are considered in the model to simulate the experimental data. It can be seen that the first peak at ~1.5 Å is attributed to the shortest six-equidistant oxygens around the Mn, Co, and Ni target absorbers occupied in the octahedral site. The second peak at ~2.5 Å is assigned to the contribution from a six-coordinated transition metal Mn/Co/Ni atom on the transition metal layer. In light of the larger radial region, the backscattering amplitudes derived from the Li and oxygen atoms are very weak due to the lighter atomic mass and lower atomic number. Moreover, the FT peaks in the $R > 4$ Å are mainly contributed from the single M−M and multiple M−M−M scattering. According to the calculation of the theoretical phase and amplitude based on the FEFF7 code, the FT peak at 4.5 Å is dominated by the contribution of 6 M−M scattering within the transition metal layer and 6 M−M scattering from two adjacent transition metal layers.[14]
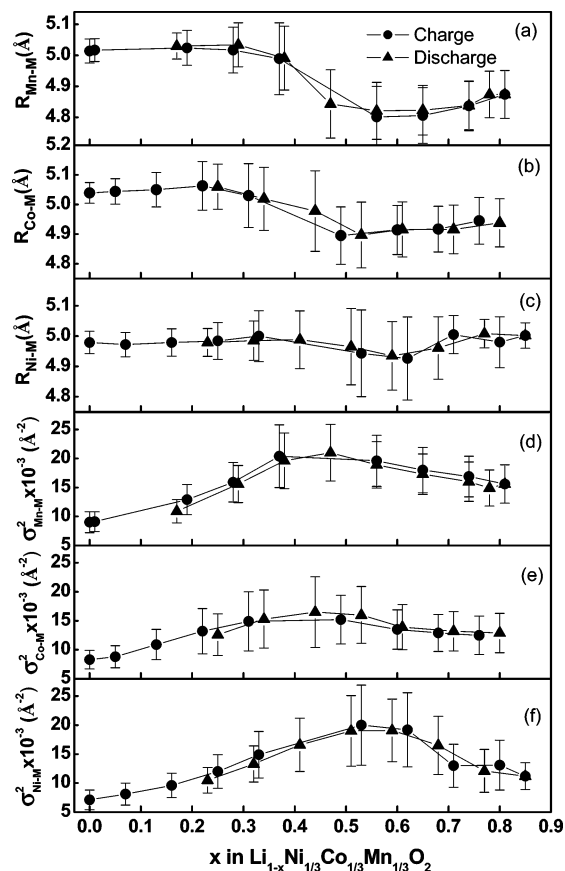
Finally, the FT peak at ~5.3 Å is contributed from the focusing effect of 12 M−M−M collinear multiple scattering, where a second scattering atom lies collinear between an emitting atom and a scatter.

The structure parameters of the local environment for the $Li_{1-x}Ni_{1/3}Co_{1/3}Mn_{1/3}O_2$ compound obtained by the curve fitting analysis are shown as a function of x in Figures 9−12. In all cases, the values of R factor for the simulated data are
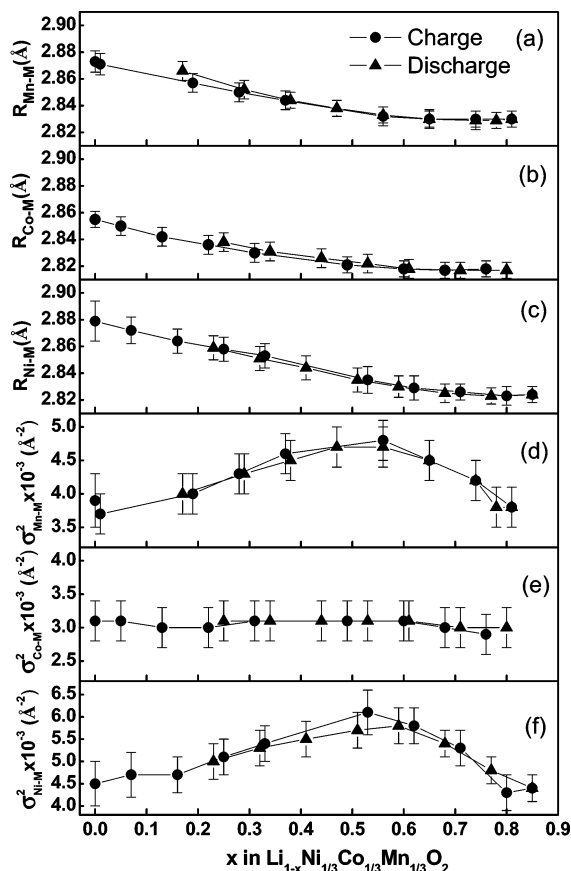
Figure 10. Structural parameter changes simulated at the second shell Mn–M, Co–M, and Ni–M for Li$_{1-x}$Ni$_{1/3}$Co$_{1/3}$Mn$_{1/3}$O$_2$ at different lithium contents during first charge and discharge cycle.

Figure 11. Structural parameters changes simulated at the third shell Mn–M, Co–M, and Ni–M for Li$_{1-x}$Ni$_{1/3}$Co$_{1/3}$Mn$_{1/3}$O$_2$ at different lithium contents during first charge and discharge cycle.

mostly less than 0.02, indicating the fitting is quite good with the known structure. Figure 9a–f shows the changes of bond length and Debye–Waller factor for the first shell Mn–O, Co–O, and Ni–O in the Li$_{1-x}$Ni$_{1/3}$Co$_{1/3}$Mn$_{1/3}$O$_2$ compound at different charging and discharging states. The structure parameters of the Mn–O, Co–O, and Ni–O shells in Li$_{1-x}$Ni$_{1/3}$Co$_{1/3}$Mn$_{1/3}$O$_2$ at different delithiated states calculated by the density functional theory have been presented in our previous paper.[10] At $x = 0$, the bond distances of the Mn–O, Co–O, and Ni–O shells in Figure 9a–c are 1.921, 1.929, and 2.045 Å, respectively. It is consistent with their atomic radius, 0.53 Å for Mn^{4+}, 0.545 Å for Co^{3+}, and 0.69 Å for Ni^{2+}. However, the experimental data are slightly less than the computational data that the bond distances of Mn–O, Co–O, and Ni–O are 1.940, 1.953, and 2.057 Å, respectively, as is often the case for computations in the generalized gradient approximation.[10] The small values of the Debye–Waller factor for Mn–O, Co–O, and Ni–O exhibited 3.0×10^{-3}, 2.3×10^{-3}, and 3.5×10^{-3} Å^2, respectively, indicate the absence of Jahn–Teller active Ni^{3+} and Mn^{3+} ions in the pristine material. As the Li ions are deintercalated from Li$_{1-x}$Ni$_{1/3}$Co$_{1/3}$Mn$_{1/3}$O$_2$ at $x = 1/3$, the bond distances of Mn–O and Co–O decrease only slightly from 1.921 to 1.914 Å and 1.929 to 1.914 Å, respectively, while the bond distance of Ni–O decreases drastically from 2.045 to 1.931 Å, indicating the Ni sites are electroactive. The Debye–Waller factor shows a maximum value of 8.5 $\times 10^{-3}$ Å^2 for Ni–O in the x range of 0.25–0.33, and that for Mn–O and Co–O shows insignificant change in the

delithiated process. It suggests that all of the Ni^{2+} ions are oxidized to Jahn–Teller active Ni^{3+} ions and the Mn and Co ions remain the in oxidation states as +4 and +3, respectively, which is consistent with the computational results. It is further confirmed that the two-step redox reaction of Ni^{2+}/Ni^{3+} and Ni^{3+}/Ni^{4+} occurs in this compound during cycle. The Mn–O and Co–O bond lengths show a small change from 1.914 to 1.906 Å and 1.914 to 1.901 Å, respectively, whereas the Ni–O bond length varies from 1.931 to 1.891 Å at the range of $1/3 \leq x \leq 2/3$. The difference of the bond distance change in Ni–O due to the different radius of Ni^{2+}, Ni^{3+}, and Ni^{4+} is 0.69, 0.56, and 0.48 Å, respectively. The computational bond distances, 1.92 Å for Mn–O, 1.90 Å for Co–O, and 1.917 Å, were found in the Li$_{1-x}$Ni$_{1/3}$Co$_{1/3}$Mn$_{1/3}$O$_2$ compound with $x = 2/3$. The significant changes of Debye–Waller factor were observed in Ni–O contribution rather than in Mn–O and Co–O contributions. The value of Debye–Waller factor for Ni–O shell decreases from 8.5×10^{-3} to 3.4×10^{-3} Å^{-2} with an increase in the x value from 0.33 to 0.67. It is in good agreement with the oxidation state of the Ni^{3+}/Ni^{4+} transition. In the reverse scan, a similar trend was found in the bond distance and Debye–Waller factor for Mn–O, Co–O, and Ni–O, implying that a decrease in Jahn–Teller active Ni^{III} concentration could reduce the occurrence of the structure distortion as lithium ion is extracted.

The variations of the bond distance and the Debye–Waller factor for the second shell Mn–M, Co–M, and Ni–M contributions are shown in Figure 10a–f as a function of x
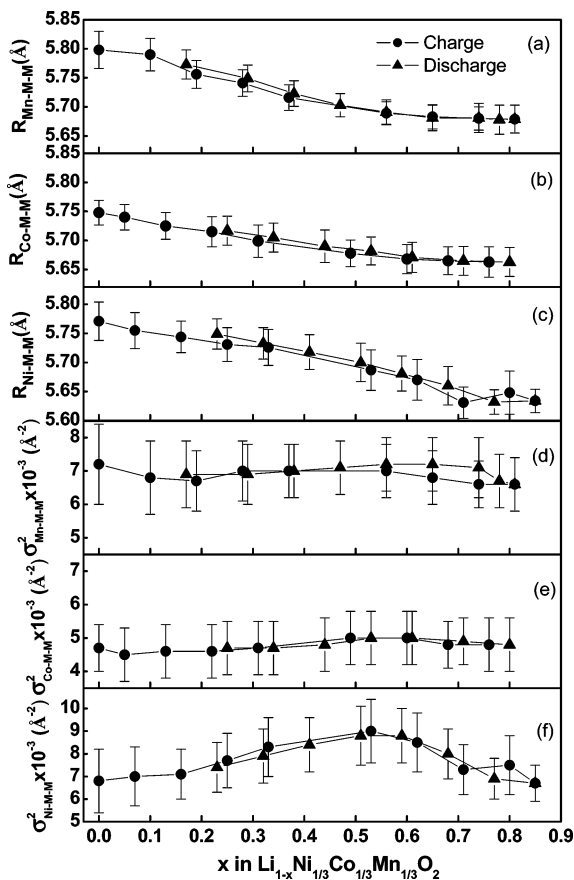
Figure 12. Structural parameter changes simulated at the fourth shell Mn−M−M, Co−M−M, and Ni−M−M for $Li_{1-x}Ni_{1/3}Co_{1/3}Mn_{1/3}O_2$ at different lithium contents during first charge and discharge cycle.

in charge and discharge. The bond distances in the second shell are similar for Mn−M and Ni−M with values of 2.871 and 2.880 Å, respectively, which is longer than that of 2.858 Å in the second shell Co−M in the pristine $LiNi_{1/3}Co_{1/3}Mn_{1/3}O_2$ compound. The Debye−Waller factor for the second shell Mn−M, Co−M, and Ni−M shown as the values of 3.8×10^{-3}, 3.1×10^{-3}, and 4.5×10^{-3} Å^{-2}, respectively, was observed in parts (d−f) of Figure 10. As the Li concentration in the material changes, the Debye−Waller factor for the second shell Mn−M and Ni−M varies with the same trend rather than that of the second shell Co−M, which has the maximum values of 3.8×10^{-3}Å^{-2} for Mn−M and 6.1×10^{-3} Å^{-2} for Ni−M at the x range of 0.5−0.6 in $Li_{1-x}Ni_{1/3}Co_{1/3}Mn_{1/3}O_2$. Moreover, the changes in the bond length for Mn−M, Co−M, and Ni−M shells are attributed to the variation of bond distance of transition metals on *ab* plane during charging/discharging process. The difference of the bond length between the starting and fully charged states is less in the Co−M shell than in the Mn−M and Ni−M shells. The variations of Debye−Waller factor and bond distance for the second M−M shells observed here provide evidence that the ordering between Ni^{II} and Mn^{IV} takes place in this compound. Because there is no long-range ordering observed in the XRD patterns, we suggest it is short-range ordering between Ni^{II} and Mn^{IV} that can only be observed by the techniques, such as XAS and NMR. Similar phenomena have also been observed in the $LiNi_{0.65}Co_{0.25}Mn_{0.1}O_2$ compound.[14] A recent computational study com-

bining density functional theory and Monte Carlo simulation shows that the ions arrange in flowerlike patterns with Li surrounded by a hexagon of Mn, which in turn is surrounded by a larger hexagon of Ni, on the layer with composition $Li_{1/12}Ni_{5/12}Mn_{6/12}$ in the $Li(Ni_{0.5}Mn_{0.5})O_2$ compound.[12] Meanwhile, NMR studies, which provide information about short-range ordering, indicate the Li ions that reside in the transition layer are preferentially surrounded by Mn ions, with significantly fewer nearest neighbor Li−Ni bonds than would be expected from a model with random distribution in the $LiNi_xMn_{(2-x)/3}Li_{(1-2x)/3}O_2$ compound.[13] Yoon et al.[22] have reported that no phase segregation takes place in the $LiNi_{1/3}Co_{1/3}Mn_{1/3}O_2$ compound from NMR and XANES studies. Although the domain of the short-range order in this compound is probably not significant enough to be observed by NMR and XANES techniques, it can be observed by EXAFS, which is more sensitive to the change of local structure. Therefore, it is suggested that short-range ordering between Ni and Mn ions occurs in this compound but is not as obvious as that in the $LiNi_xMn_{(2-x)/3}Li_{(1-2x)/3}O_2$ compound.

The bond length and Debye−Waller factor changes for the third shell Mn−M, Co−M, and Ni−M in $Li_{1-x}Ni_{1/3}Co_{1/3}Mn_{1/3}O_2$ at the different charging and discharging states are given in parts (a−f) of Figure 11. Significant decreases in the bond lengths and increases in the Debye−Waller factor for the third shell Mn−M, Co−M, and Ni−M contributions were observed with increasing the x value from 0 to 0.60 on delithiation. However, small increases in the bond length and decreases in the Debye−Waller factor for the third shell Mn−M, Co−M, and Ni−M contributions found at the x value from 0.6 to 0.85 on delithiation. The Debye−Waller factors for the third shell Mn−M, Co−M, and Ni−M have maximum values appearing at $x = 0.6$.

The changes of the bond length and Debye−Waller factor for the fourth shell Mn−M−M, Co−M−M, and Ni−M−M in the $Li_{1-x}Ni_{1/3}Co_{1/3}Mn_{1/3}O_2$ compound at the different charging and discharging states are shown in parts (a−f) of Figure 12. As it can be seen, the change in the bond length for the Ni−M−M and Mn−M−M contribution is larger than that for the Co−M−M contribution, because the redox reactions of Ni^{2+}/Ni^{3+} and Ni^{3+}/Ni^{4+} take place during cycle and the short-range ordering between Ni and Mn on the *ab* plane in this compound.

Conclusion

The electronic transitions and the local structure of the $Li_{1-x}Ni_{1/3}Co_{1/3}Mn_{1/3}O_2$ compound were investigated by in-situ X-ray absorption spectroscopy upon charge and discharge. The XANES data demonstrate the oxidation states for Mn, Co, and Ni absorbers are +4, +3, and +2, respectively, in the pristine $Li_{1-x}Ni_{1/3}Co_{1/3}Mn_{1/3}O_2$ compound. During lithiation and delithiation cycle in the potential range of 3−4.5 V, an intermediate state of Ni^{3+} is observed from the variation of bond change and the Debye−Waller factor for the M−O shell. A two-step redox reaction involving Ni^{2+}/Ni^{3+} and Ni^{3+}/Ni^{4+} takes place during cycle,

(22) Yoon, W.-S.; Grey, C. P.; Balasubramanian, M.; Yang, X.-Q.; Fischer, D. A.; McBreen, J. *Electrochem. Solid-State Lett.* **2004**, *7*, A53.

but the oxidation states of Mn and Co remain as Mn^{IV} and Co^{III}, respectively. It suggests that that the oxygen, rather than the transition-metal ions (Ni, Co, and Mn), functions as the electron donor at the end of charge. The significant change in the bond length and Debye−Waller factor for the second shell M−M arises mainly from the generation and reduction of the Jahn−Teller active Ni^{III} sites. The trends of the variations for the bond length and Debye−Waller factor for the second shell Mn−M and Ni−M contributions are significant and similar, suggesting the short-range ordering between Ni^{II} and Mn^{IV} may take place in this compound.

However, this kind of short-range ordering is probably not significant enough to be observed by NMR.